Journal of Non-Crystalline Solids 273 (2000) 81–93

# Surface crystallization and texture in cordierite glasses

N. Diaz-Mora [a], E.D. Zanotto [a,*], R. Hergt [b], R. Müller [c]

[a] *Department of Materials Engineering – DEMa, Vitreous Materials Laboratory – LaMaV, Federal University of São Carlos – UFSCar, 13565-905 São Carlos – SP, Brazil*

[b] *Institute for Physical High Technology – IPHT, P.O. Box 100 239, D-07702 Jena, Germany*

[c] *Federal Institute for Materials Research and Testing, BAM Branch Adlershof, Rudower Chaussee 5, D-12489 Berlin, Germany*

**Abstract**

Systematic work was carried out at 860°C ($T_g \sim 800$°C) on the crystal growth of a high-quartz solid solution phase (μ-cordierite), which crystallizes on solid impurities on the surface and in the volume of the same cordierite glass sample. Crystal growth velocities were determined for three different growth fronts: (I) crystals that nucleated on solid inclusions existing in the glass interior and grew radially; (II) isolated crystals that nucleated on the external sample surfaces and grew with the fast axes parallel to the surface, and (III) crystals that nucleated on the external surfaces and grew towards the specimen center, spontaneously forming a textured surface layer. The crystal growth velocities of the three fronts were equal. We conclude, therefore, that the mechanisms of molecular transport at the crystal–liquid interface (or interfacial rearrangement) for crystal growth on the surface and in the interior of cordierite glass are similar. X-ray diffraction investigations have shown that, in case (III), a fiber texture is spontaneously formed with preferential alignment of the $c_0$-axis of the grains normal to the growth front. The texture dispersion angle decreases towards the interior of the glass, in accordance with evolutionary microstructural models. The apparent induction times (≈2 h) for growth of internally nucleated crystals, case (I), and (≈3 h) for the isolated surface crystals, case (II), indicate that different nucleation sites have caused heterogeneous nucleation on the surface and in the glass interior. The long induction time for growth of the textured surface layer (≈11 h) is due to a succession of two different growth modes that form the texture in this glass. 

## 1. Introduction and objectives

Surface crystallization of glass is scientifically relevant and has a number of technological implications [1,2]. The crystal nucleation and growth kinetics of some of the crystalline phases that occur on the surface of nearly stoichiometric cordierite glasses, $2MgO \cdot 2Al_2O_3 \cdot 5SiO_2$, have been investigated recently [3–6]. This paper describes original research on the crystal growth behavior of a metastable high-quartz solid solution phase ('μ-cordierite') that crystallizes from the surface and from impurities existing inside a cordierite glass, providing a unique opportunity to compare the *growth kinetics* of the same crystal phase on the surface and in the interior of the same parent glass. These findings allow us to verify whether the molecular transport mechanism (or interfacial rearrangements) controlling crystal growth in the glass interior is similar to those on the glass surface.

Additionally, we perform a systematic study to test the possibility of *texturing* of the resulting microstructure (texture is defined as a deviation from the random orientation of an ensemble of

* Corresponding author. Tel.: +55-16 271 4871; fax: +55-16 261 5404.

*E-mail address:* dedz@power.ufscar.br (E.D. Zanotto).

0022-3093/00/$ - see front matter 
PII: S0022-3093(00)00147-2

crystallites). In the often-occurring case of fiber texture, there is a tendency for the grains to align parallel to a particular crystallographic axis. Most of the properties of crystalline materials of technical interest, such as mechanical, electrical, magnetic or thermal properties, are strongly influenced by texture-related anisotropy. Additionally, several processes of phase formation, such as solid-state processes of plastic deformation and recrystallization, are accompanied by texture generation [7]. One of the most successful methods to obtain a defined crystallographic orientation in glass-ceramics is solid-state epitaxy. Headley and Loehman [8], for instance, demonstrated that a $Li_2O$–$Al_2O_3$–$SiO_2$–$P_2O_5$ glass-ceramic crystallizes by epitaxial growth in the glass volume, while Liu et al. [9] and Selvaraj et al. [10] investigated the role of epitaxy on the crystallization of albite glass, $NaAlSi_3O_8$. Glass-ceramics with oriented crystals can also be formed by extruding glasses [11–13]. Oriented $Li_2O \cdot 2SiO_2$ glass-ceramics in a temperature gradient and crystallization of glass fibers were produced by Engel and Frischat [14].

It is also known that spontaneous preferential growth from the external glass surfaces may occur in certain situations, leading to textured microstructures and yielding properties that are peculiar to some glass-ceramics. For example, textured $Li_2O \cdot 2SiO_2$ glass-ceramics present interesting pyroelectric properties [15]. However, there is a paucity of information on spontaneous preferred orientation of crystals formed by devitrification. Thus, another goal of this research is to investigate the possible *spontaneous orientation* of the crystallized layer to aid in the interpretation of the crystal growth behavior of the distinct growth fronts in cordierite glass.

Finally, we present and discuss a peculiar aspect of the behavior of the *induction times* for crystal growth of the different fronts focused on in this study.

## 2. Materials and methods

The cordierite glass, code GM30870, used in this study was supplied by Schott Glaswerke. Its analyzed composition was 52.3 wt% $SiO_2$, 33.2 wt% $Al_2O_3$, 14.6 wt% MgO, which differed a little from the stoichiometric composition (51.3 wt% $SiO_2$, 35.0 wt% $Al_2O_3$, 13.7 wt% MgO). Additionally, some measurements were made of a glass having an almost stoichiometric composition that deviates less than 0.5% from the ideal composition for each component.

The specimens were ground with SiC water slurries on plane brass tools and polished to optical grade with a $CeO_2$ slurry (to determine the crystal growth rate) or $CeO_2$ and diamond paste (for texture measurements). The polished samples were heat-treated in air in an electric furnace with a temperature stability of $\pm 2$°C. The treatment temperature was 860°C ($T_g \sim 800$°C) with time periods of up to 80 h. To examine the texture of the crystalline surface layer, some samples were ground with SiC and polished with $CeO_2$ before thermal treatments at 860°C and 910°C. The treated samples were cut, polished and then etched with a 1 vol.% HF solution and examined with a scanning electron microscope (SEM). Samples treated at 910°C for 3 h were broken and viewed sideways in the SEM.

The heat-treated samples were observed in an optical microscope (Jenapol Carl Zeiss/Jena), using polarized transmitted light. In every case, a 1:0.01 mm scale was photographed under identical experimental conditions. To describe the crystal growth of the internal crystals, the length of one crystal (the largest found), $L_v$, was followed throughout the series of cumulative thermal treatments (I). For the isolated surface crystals, one-half of the maximum length, $L_1$, of the largest crystal found in a given set of micrographs was chosen for each measurement (II). Finally, the thickness of the compact crystalline surface layer, $L_s$, was measured (III). The crystal dimensions indicated in Fig. 1 were measured with an accuracy of $\pm 1$ μm.

The preferential orientation of the crystallites on the surface and the change in texture degree within the crystallized surface layer were investigated by X-ray diffraction, using Cu-K$\alpha$ radiation on a X'Pert (Philips) diffractometer equipped with an Euler cradle. To take a pole figure, the detector was fixed at the Bragg angle of a special set of planes to be investigated. The diffraction space was

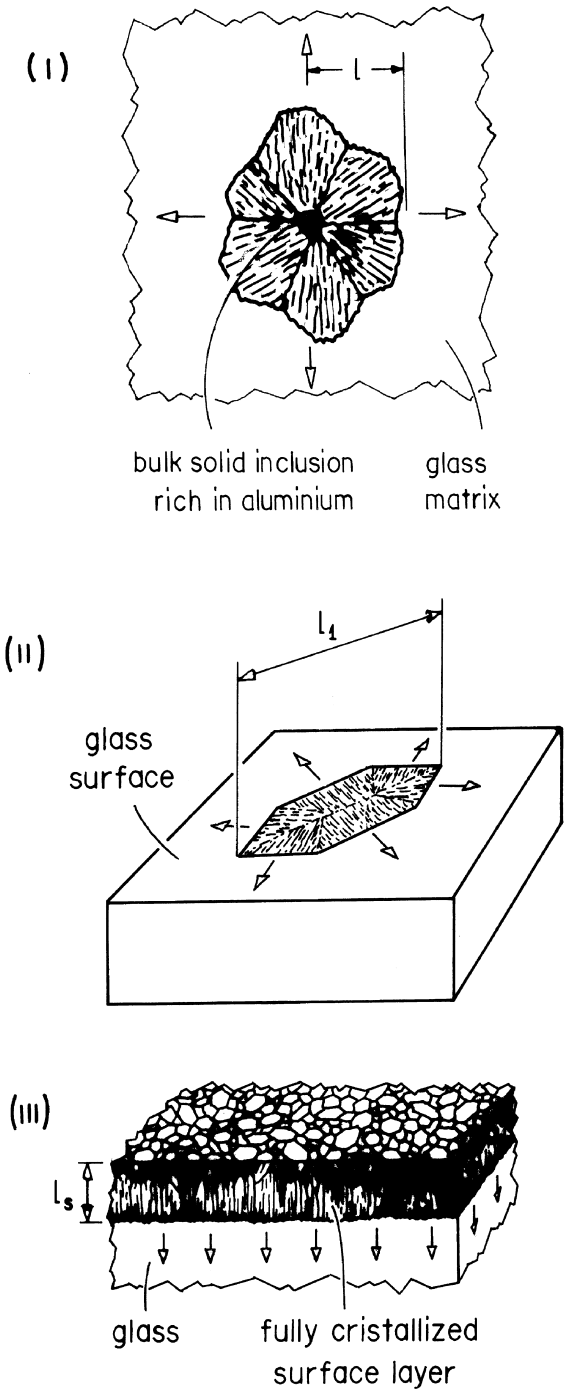


Fig. 1. Illustration of the crystal lengths in crystallized cordierite glass: case (I), length of a petal of rosettes, $L_v$; case (II), the largest length of elongated hexagons, $L_1/2$; case (III), crystal surface layer, $L_s$.

then scanned by rocking the sample stepwise about two orthogonal axes, $\Psi$ (normal to the diffraction plane) and $\Phi$ (normal to the sample surface). The resulting diffracted beam intensity was represented on a contour plot – the so-called pole figure.

Measurements by energy dispersive X-ray spectroscopy (EDS) were made using equipment Link QX2000 coupled to a scanning electron microscope (Carl/Zeiss DSM970).

## 3. Results

### 3.1. Crystal morphology

Fig. 2(a) shows hexagonal crystals of different shapes (regular and elongated), growing from a polished sample surface, as the dominating morphology type. Additionally, crystals having the same morphology grew from some solid inclusions randomly distributed in the interior (Fig. 2(b)). After some growth, these crystals formed 'rosette'-like, almost spherical crystals.

EDS measurements have shown that nucleating solid inclusions are rich in aluminum (Fig. 3). Such particles are probably $Al_2O_3$ resulting from incomplete dissolution of this oxide during melting. Fig. 3 also shows EDS measurements performed on a rosette petal and in the glass matrix, which had essentially identical compositions. This finding, coupled to previous infrared spectroscopy, Raman microprobe analysis and X-ray diffraction measurements [5,6,16,17], indicates that all the crystals observed are μ-cordierite. This phase usually occurs as the primary phase during cordierite glass crystallization [18]. Thus, the different shapes of μ-cordierite surface crystals, illustrated in Fig. 2, are attributed to different crystal orientations with respect to the surface plane.

### 3.2. Crystal growth kinetics

The glass sample under study allowed us to measure the crystal growth rates of μ-cordierite for three different cases: (I) crystals nucleated at solid inclusions in the interior of the glass, growing radially and forming rosettes, (II) isolated surface crystals nucleated at the external surface, growing

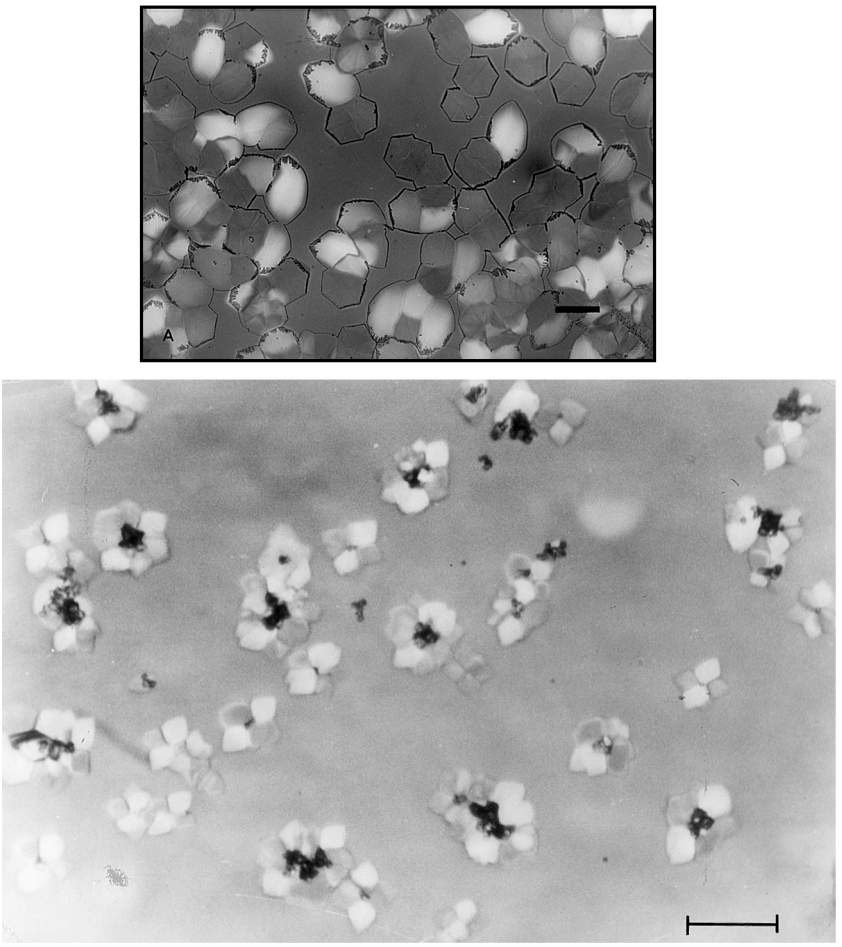


Fig. 2. Typical optical micrographs (polarized transmitted light) of some morphologies observed in GM30870 cordierite glass samples: (a) regular and elongated hexagons on the glass surface (⟼⟻ = 20 μm). Thermal treatments at 890°C for 1 h 15 min and at 925°C for 15 min; (b) rosettes in the interior of the glass after thermal treatment at 910°C for 3 h (⟼⟻ = 50 μm). Almost all crystals have a solid inclusion in their center.

parallel to the surface, and (III) a compact crystalline surface layer growing into the interior (see Fig. 1). Crystal size data are given in Fig. 4, where the largest radius of the rosettes, $L_v$ (□, case I), the half-length (major axis) of the largest crystal on the glass surface, $L_1$ (•, case II), and the surface layer thickness, $L_s$ (△, case III) are shown. The corresponding crystal growth velocities, $U$ (± standard error) and induction periods obtained by a least-squares fit, are shown in Table 1.

In these three cases, the crystal growth velocities were equal within the error limits. The average, $3 \times 10^{-10}$ m/s (0.018 μm/min or 1.08 μm/h), agrees with previous data for the growth velocity of μ-cordierite (≈0.02 μm/min) at the same temperature in the stoichiometric glass [19].

Fig. 4 also shows intercepts on the time axis, indicating the existence of apparent 'induction periods' for crystal growth in the GM 30870 sample. There is an intriguing difference between these induction periods: $\tau_{AI} = 1.7$ h, $\tau_{AII} = 2.9$ h, and $\tau_{AIII} = 11$ h.

Fig. 5 shows a similar situation for the stoichiometric glass at $T = 980$°C. The growth rate of

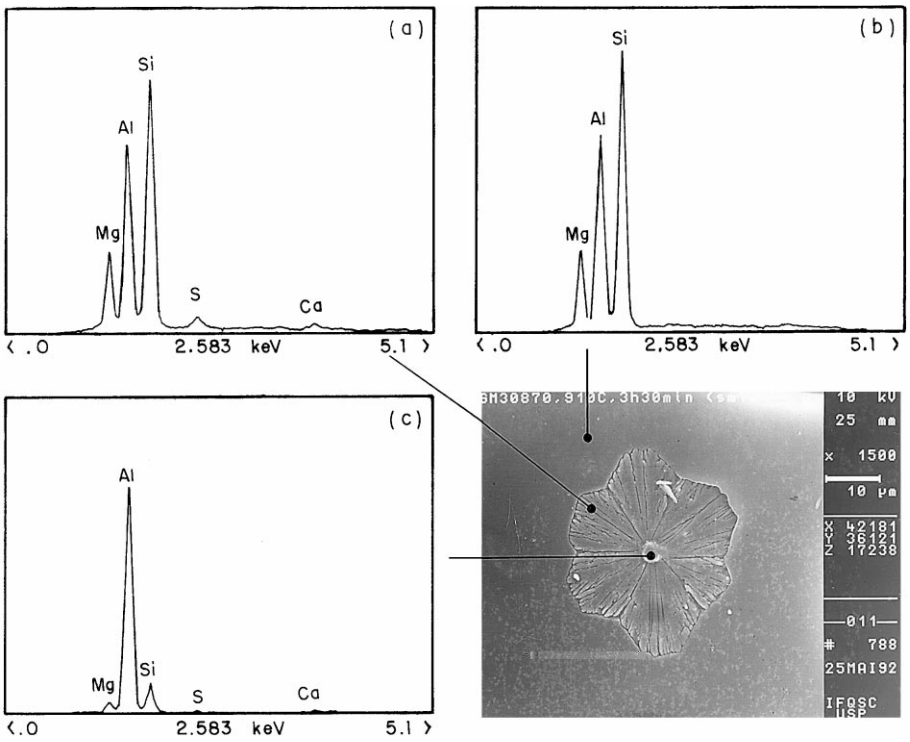


Fig. 3. EDS of: (a) solid inclusions in the interior of the GM30870 cordierite glass; (b) a petal of a rosette and (c) the glass matrix.

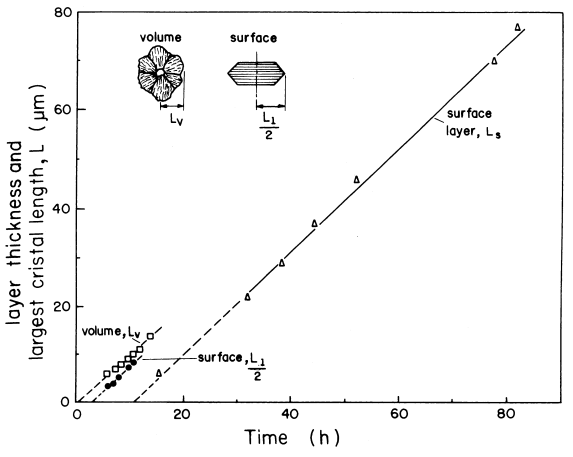


Fig. 4. Time dependence of crystal growth in GM30870 cordierite glass samples treated at 860°C: □, largest length of internally growing rosette-like crystals (case I); •, largest hexagonal crystals on the surface (case II, $L_1/2$); △, thickness of the surface layer. The error bars are about equal to the symbol sizes.

the crystallized surface layer from a SiC-ground surface is compared to that of a fractured surface. The crystal growth rate is about $7.8 \times 10^{-7}$ m/s (that is 1.3 μm/min or 78 μm/h) in both cases. However, while $\tau$ is almost zero for the ground surface, $\tau \approx 2$ h for the fractured surface.

### 3.3. Texture of the crystalline surface layer

#### 3.3.1. Isolated surface crystals

Top-view observation of isolated surface crystals by transmitted light microscopy indicates that the apparent crystal shapes consist only of regular or elongated hexagons and, therefore, crystal orientation is *not* random. The ratio of the numbers of elongated to regular hexagons, *e/r*, increases with increasing annealing temperature, e.g., $e/r = 0.1$ (870°C, 3.5 h, $L_1 \approx 3$ μm), $e/r = 1.0$ (950°C, 0.5 h in vacuum, $L_1 \approx 40$ μm), and

Table 1
Crystal growth velocities and induction periods of μ-cordierite in GM 30870 glass at 860°C taken from Fig. 4

| Growth front | Crystal growth velocity (m/s) | $\tau$ (h) |
|---|---|---|
| (I) Rosettes in the bulk | $U_v = (3.2 \pm 0.2) \times 10^{-10}$ | $1.7 \pm 0.2$ |
| (II) Elongated hexagons on the surface | $U_l = (2.9 \pm 0.2) \times 10^{-10}$ | $2.9 \pm 0.2$ |
| (III) Crystallized surface layer | $U_s = (3.1 \pm 0.1) \times 10^{-10}$ | $12 \pm 1$ |

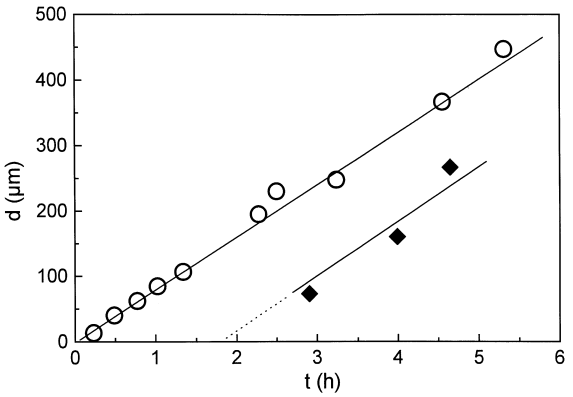


Fig. 5. Thickness of the compact μ-cordierite surface layer in stoichiometric glass as a function of time for $T = 980$°C. ○, SiC-ground glass surface, ◆, fractured glass surface. The error bars are smaller than the symbol sizes.

$e/r = 1.8$ (950°C, 40 min, $L_1 \approx 40$ μm). Large crystals ($L_1 > 50$ μm), growing from fractured or polished sample surfaces with low-density of nucleation sites ($N_s < 10^{-6}$ μm$^{-2}$), have an elongated shape in almost every case. Optical interference surface scans of polished and then thermally treated sample surfaces indicate that this orientation might be caused by surface tension phenomena [20]. As illustrated in Fig. 6(a), the regular hexagons were drawn into the sample interior, causing local depressions of the glass surface (up to 40 nm), while most elongated crystals stand out (up to 60 nm). These effects show that crystal orientation can change during crystal growth, depending on the crystal/melt interfacial energies for different crystal faces. As the crystal growth in this study took place well above $T_g$, the viscosity ($10^{9.9}$ Pa s) was small enough to allow the crystal orientation to change with time. This observation is confirmed by the smooth, wavy profile of glass surfaces after crystallization treatments. This process should affect the ratio of regular to elongated crystals for surfaces having different nucleation site densities.

X-ray diffraction patterns ($\theta/2\theta$ scans) of as-annealed glass surfaces are shown in Fig. 7. The glass specimens were partly devitrified by annealing at 860°C for 80 h (~75 μm thick layer). The samples differ in their pre-annealing treatment. Sample (a) was diamond-polished while sample (b) was polished with cerium oxide. A comparison of experimental diffraction patterns with ICDD standard files show that the only crystalline phase appearing after annealing diamond-polished samples (Fig. 7(a)) is μ-cordierite. The diffraction line intensities shown in Fig. 7 deviate slightly from the typical intensities for a random grain distribution (ICDD database). Hence, due to the X-ray penetration into the sample, this result does not confirm the preferential orientation of the outer surface layer. In the case of the $CeO_2$-polished surface (Fig. 7(b)), an additional phase ('$x$-phase' $-2\theta = 12.46°$ and 25.02°) appears. Pole figures taken with the diffraction line at 12.46° show that this second phase is also textured.

### 3.3.2. Impingement of surface crystals and further growth

During prolonged growth ($t > \tau$) of the isolated surface crystals, a compact layer is formed and the degree of crystal orientation increases due to impingement of non-perpendicular crystals and the survival of perpendicular growing crystals [5–7,21]. A typical micrograph is shown in Fig. 8(a). A tendency for crystal alignment near the interface is observed. Fig. 8(b) shows a sample from which the crystallized surface layer was partly removed by grinding and polishing. The residual glass matrix can be observed in some regions, but the texture is evident by visual inspection.

To investigate the dependence of texture formation on the depth, $z$, towards the interior, we

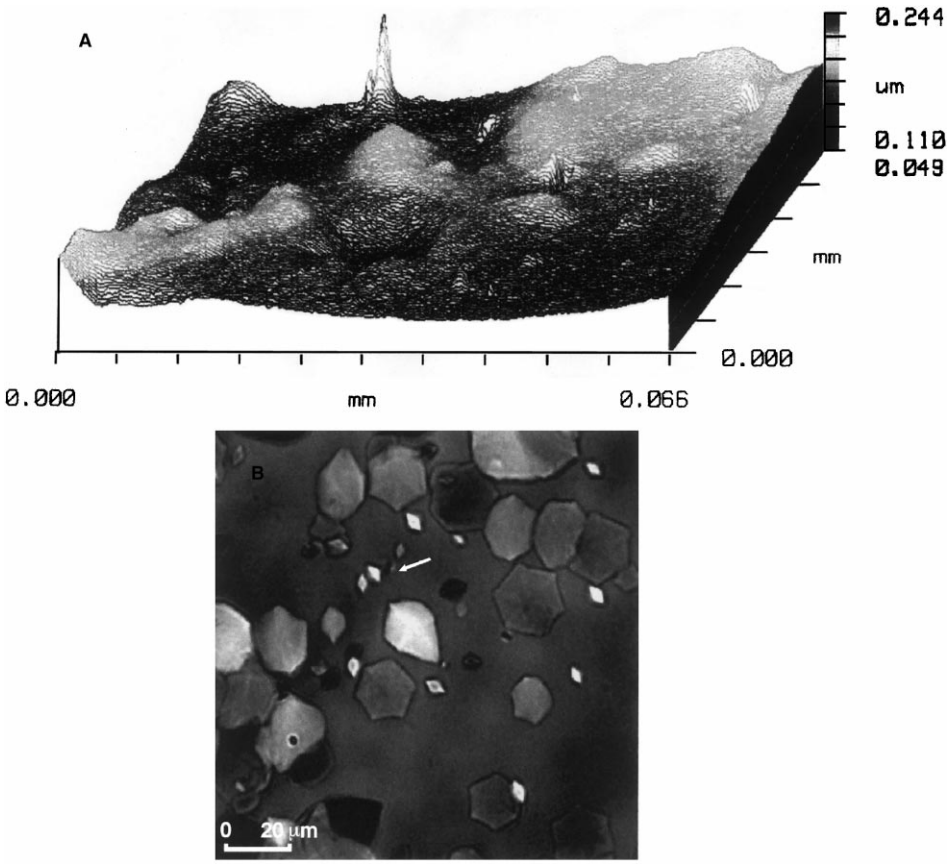


Fig. 6. (a) Surface profile map obtained by an optical interference microscope. Stoichiometric cordierite glass surface polished and then annealed at 950°C for 1 h, taken from [20]. (b) Transmitted light top-view micrograph showing the same sample region. The arrow marks a dust particle appearing as a sharp peak in the surface profile (a).

removed several layers in steps of about 10 μm, followed by (pole-figure) X-ray diffraction measurements. Grinding with SiC and subsequently polishing with diamond paste led to repeated thinning of the surface layer. The removal of a 10 μm thick layer revealed an appreciable increase of the texture. Only a few lines remained in the diffraction pattern, as can be seen by comparing Fig. 9 with Fig. 7. Reflections from prism planes are absent.

To examine the texture in more detail, pole-figures were taken with the (1 0 1) reflection, the results of which are shown in Fig. 10. In this figure, the intensity of the (1 0 1) reflection is shown by different gray areas (range of kilo counts) as a function of $\Phi$ [1] and $\Psi$. Fig. 10 shows a ring-shaped maximum of the (1 0 1) intensity. No effect of $\Psi$ is evident, confirming the observation that the elongated hexagons are preferentially oriented (with their $a_0$-axis) in top view micrographs. However, with respect to $\Psi$, a broad maximum of the (1 0 1) intensity is evident at 30° (see also Fig. 11, e.g., for $z = 20$ μm). This maximum indicates the preferred

[1] $\Phi$ gives the rotation angle of an ideal perpendicular surface crystal around its $c$-axis. The latter axis stands out on the paper plane in Fig. 10. $\Psi$ gives the tipping angle of the c-axis of that perpendicular crystal against the X-ray reflection plane. $\Psi$ ranges from zero, at the center of the pole figure, to 90°, the outer circle.

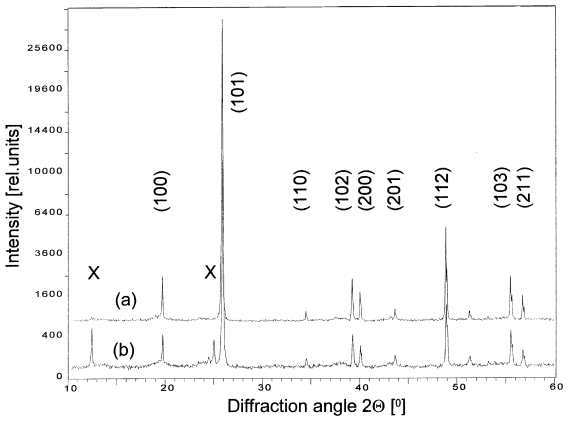


Fig. 7. X-ray diffraction pattern of the GM30870 cordierite glass sample, polished with (A) diamond and (B) cerium oxide, and treated at 860°C for 80 h.

orientation of hexagonal $c_0$-axes normal to the growth front of the crystallizing surface layer. However, there is an angular spread of grain axes of about 30° deriving from the half-width of the ring in Fig. 10.

The texture of the initial surface crystal layer ($z = 0$) and after the removal of 20 and 40 μm is compared by $\Psi$-scans in Fig. 11. The angular width at half maximum intensity (after correction for background) is taken as a measure of texture spread and is plotted in Fig. 12, as a function of the depth of the removed layer. We observe that the texture improves with increasing depth into the surface layer down to a critical depth, after which it deteriorates until the bulk glass is met. Obviously, the texture develops during grain growth towards the sample's interior.

## 4. Discussion

### 4.1. Texture formation on surface crystallization

It is well known from various film deposition studies that texture develops during growth of granular films (e.g., [21,22]). The underlying mechanism, often called 'survival of the fastest', may be related to several evolutionary processes [21,22]. In the present case, a plane crystallization front of many crystalline grains moves inward in

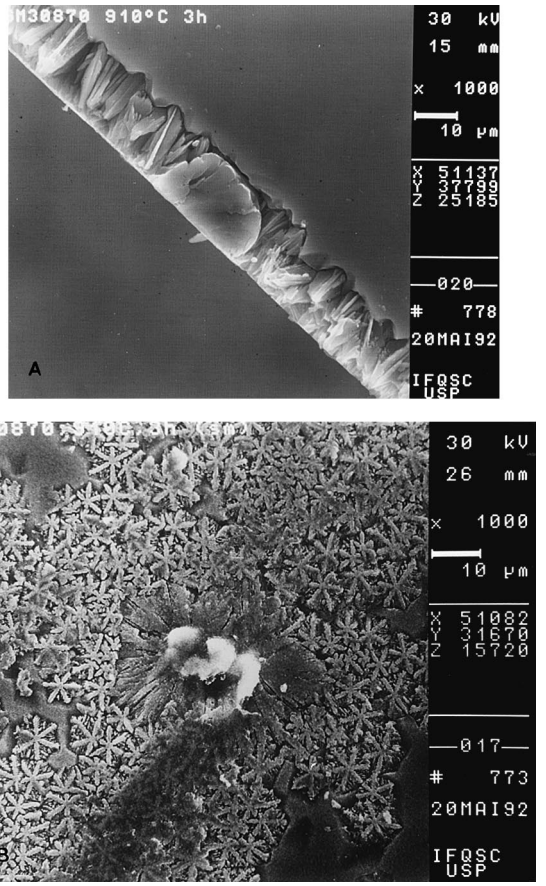


Fig. 8. SEM Micrographs of the GM30870 cordierite glass treated at 910°C for 3 h, etched with an HF 1 vol. solution: (a) profile view of crystallized surface; (b) top view of a partially removed surface layer. An internal crystal grown on a solid inclusion is shown in the center.

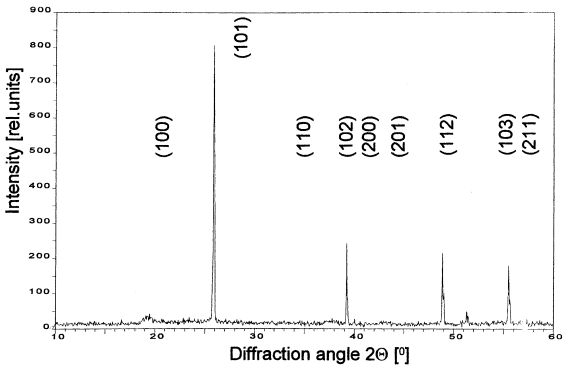


Fig. 9. X-ray diffraction pattern of the sample shown in Fig. 8(a) after removing a 10 μm thick layer.

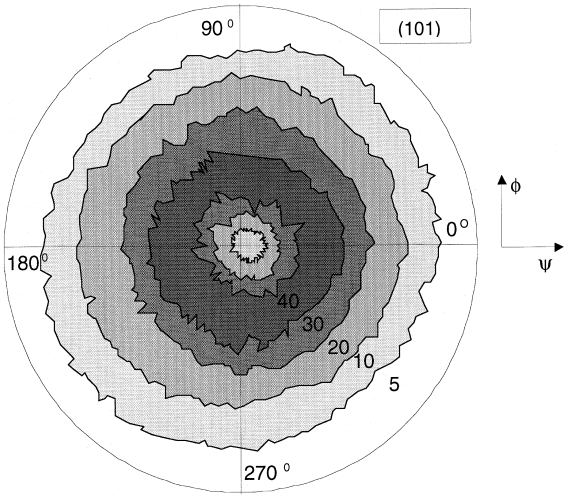


Fig. 10. (1 0 1) pole figure of the sample shown in Fig. 9 (the diffraction intensity is given in kilo counts on the contour lines).

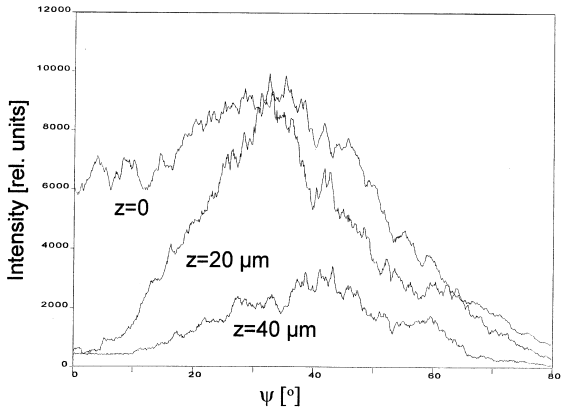


Fig. 11. X-ray $\Psi$-scans after removing layers of different $z$ thicknesses from the as-annealed glass surface.

the glass. The grains of this layer grow in competition with each other, similar to the grain growth of a polycrystalline film on a substrate. The texture evolves in such a way that the grains with the fast growing $c_0$-axis orientation perpendicular to the growth front are preferentially selected.

Such evolution is clearly shown by the X-ray results of this study. Typically, in the surface scan ($z = 0$) in Fig. 10, besides growth of the textured part of the layer, a grain population with random orientation is still present, as indicated by a non-

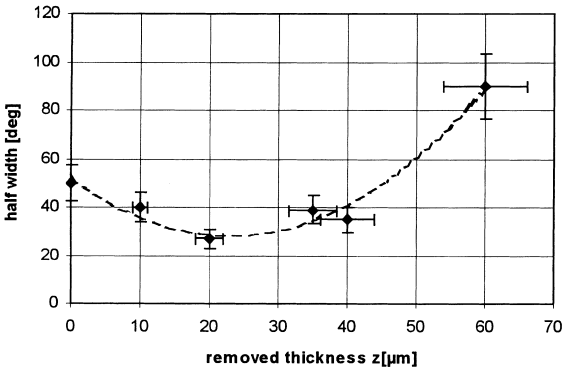


Fig. 12. Dependence of the orientation spread (FWHM) on the thickness of the removed layer from the as-annealed glass surface.

vanishing diffraction peak at $\Psi = 0$. A peak in the orientation distribution is observed at $z = 20$ μm. Transition to the interior occurs close to the front of the crystallized layer (near $z = 60$ μm).

### 4.2. Crystal growth kinetics

To compare the crystal growth kinetics of the three different cases, we assume that the liberation of latent heat at the growth front does not alter the interface temperature owing to the slow growth velocities ($\sim 1$ μm/h) at the high undercooling chosen for this study. Moreover, there is no substantial compositional difference between the growing phase and the parent glass. Under these circumstances, interface-controlled growth should prevail over long-range diffusion. Thus, the atomic attachment rate of 'growth units' to the crystal–melt interface, characterized by an effective diffusion coefficient, $D$, should control the crystal growth velocity, $U$, according to Eq. (1)

$$U = Z(D/\lambda)[1 - \exp(-|\Delta G|/RT)], \quad (1)$$

where $Z$ is the fraction of atomic sites at the crystal interface available for attachment, $\lambda$ the jump distance, $\Delta G$ the thermodynamic driving force per mole, $R$ the gas constant and $T$ the absolute temperature [23].

As the same phase crystallizes on the glass surface and in its interior, all the parameters of Eq. (1) should be identical except the effective

diffusion coefficient, which could vary from surface to bulk diffusion. In principle, we expect that surface transport controls crystal growth in situation (II), where the isolated crystals grow with the fast axis parallel to the surface, while bulk diffusion controls growth in situations (I) and (III).

It is well known that surface diffusion is faster than bulk diffusion in a variety of materials; thus, the growth rate could be expected to be largest in situation (II). However, the deviation of near-surface properties (e.g., composition) are known to be restricted to a layer of the order of *nanometers*, e.g., [24]. Thus, the growth of any crystal of a size detectable by optical microscopy should be determined by the bulk properties. This prediction is confirmed by the similar growth rates obtained from Fig. 4.

Growth velocity generally depends on the crystallographic direction of a crystal. However, as shown in the previous section, in all three cases chosen for the present study – (I) the fastest growing crystal within a rosette-like aggregate around inclusions in the glass interior, (II) the fastest elongated hexagon selected by the human operator, or (III) the fastest growing crystals within the surface layer, spontaneously selected by impingement phenomena – the crystal growth rate data refer to the same crystal face and orientation and, therefore, their kinetics can be compared.

Three (apparent) induction times for crystal growth at 860°C, $\tau_A$, are shown in Fig. 4: $\tau_{AI} = 2$ h (rosette-like crystals in the glass interior), $\tau_{AII} = 3$ h (isolated crystals at the surface), and $\tau_{AIII} = 11$ h (compact crystal surface layer). Generally, several time-lag effects can contribute to $\tau_A$

$$\tau_A = \tau_b + \tau_g + \tau_s, \tag{2}$$

$\tau_b$ is the time required to form a detectable number of critical nuclei, $\tau_g$ the time necessary for a critical nucleus to achieve (almost) constant growth velocity [25] and $\tau_s$ is the time required for the surface layer to reach steady-state growth conditions (e.g., to form a continuous layer having a texture). The time required for a growing crystal (having a constant growth velocity) to reach a detectable size does not influence the extrapolated intercept of the linear $L(t)$ plot to $t = 0$.

### 4.3. Time lag for nucleation, $\tau_b$

Crystal growth should start immediately after the first – or at least a detectable number of – critical nuclei are formed, even before steady-state nucleation is established. However, this time, $\tau_b$, is not known. Hence, to a first approximation we could replace $\tau_b$ by its upper bound $\tau, (\tau > \tau_b)$, where $\tau$ gives the induction period for nucleation. $\tau$ can be approximated by [26]

$$\tau \approx \lambda^5 \sigma N_A^2 \eta / Z \Delta\mu^2, \tag{3}$$

where $\lambda$ is the intermolecular distance, $\sigma$ the nucleus/liquid interfacial energy, $N_A$ the Avogadro number, $\eta$ the viscosity, $Z < 1$ the steric factor and $\Delta\mu$ is the thermodynamic driving force for crystallization.

Eq. (3) gives $\tau \approx 1$ s for $T = 860$°C and $Z = 1$ if one uses typical physical parameters for stoichiometric cordierite glass [27] ($\lambda = 2 \times 10^{-10}$ m, $\sigma = 0.193$ J/m$^2$, $\eta(860°C) = 10^{10}$ Pa s, $\Delta\mu(860°C) = 21$ kJ/mol). This $\tau$ is negligible. However, the time lag of nucleation *calculated* from the size distribution of μ-cordierite crystals in [19,28] shows that $Z \approx 10^{-4}$ ($\tau \approx 3$ h) must be used to achieve the best fit of the experimental time-lag data. In an independent study, $Z \approx 10^{-4}$ and $Z \approx 10^{-2}$ were reported for the nucleation of $Li_2O \cdot 2SiO_2$ crystals in lithium aluminosilicate and $Li_2O \cdot 2SiO_2$ melts, respectively [26]. This estimate thus shows that $\tau$ has the same order of magnitude ($\approx$ 2–5 h) and covers the intercepts in Fig. 4 for case (I) and (II). The smaller $\tau$ observed for the growth of internally nucleated crystals (rosettes, case (I)) may be caused by a greater nucleation efficiency of the internal solid particles. In this case, $\tau$ would be reduced to $\tau^* = \tau\Psi^{1/2}$ [23], where $\tau$ is the homogeneous nucleation time lag, $\tau^*$ is the time lag for heterogeneous nucleation and $\Phi$ is the substrate activity.

### 4.4. Time lag for constant crystal growth, $\tau_g$

Despite the observed linear growth of large crystals shown in Fig. 4, a non-linear growth is to be expected for small (critical size) crystals. Thus, a certain period of time, $\tau_g$, is required to attain an

(almost) constant crystal growth velocity. Assuming the continuous ballistic model for nuclei growth, which predicts a size-dependent growth velocity, Weinberg [25] demonstrated that crystal size is not a simple linear function of time. Instead, Eq. (4) gives an approximation

$$R(t) = Ut - r^* \ln(W^*/kT) - r^* \ln(t/\tau), \quad (4)$$

where $U$ is the experimental crystal growth velocity normally observed from optical microscopy, $W^*$ the free energy barrier to form a critical nucleus, $r^*$ its size and $\tau$ is the transient time of nucleation.

To estimate the effect of size-dependent growth, Eq. (4) was used with real parameters for the stoichiometric cordierite glass ($r^* = 2 \times 10^{-9}$ m, $W^* = 3.2 \times 10^{-18}$ J, $\tau = 10^5$ s) calculated from calorimetric [27] and crystal size distribution measurements [19]. Additional calculations were made for 800°C, 900°C, and 950°C using $\tau = 10^5$ s and $\tau = 1$ s (see Eq. (3) for $\tau$). However, no detectable time lag for growth could be found in any of the cases. To obtain a detectable time lag, an unrealistically large $r^*$ must be assumed (for instance $r^* > \approx 100$ nm). Thus, for the present case, the effect of size-dependent growth phenomena can be reasonably excluded and $\tau_g$ can be neglected.

According to [25], $\tau_g$ should be negligible for $W^*/kT > 200$. Indeed, for cordierite glass at 860°C, using $W^*/kT = 16\pi\alpha^3 \Delta H_f T_f^2/3(T_f - T)^2.N_A$, with $\alpha = 0.5$, $\Delta H_f = 180$ kJ/mol, $T_f = 1623$ K, one has $W^*/kT \sim 440$. Using lower bound for these parameters yields $W^*/kT \sim 220$. Therefore, these calculations confirm the previous estimates of $\tau_g$.

### 4.5. Time lag for continuous surface layer growth, $\tau_s$

It is known, from previous studies [29], that the nucleation density for the *polished* glass surfaces under study is about $\approx 10^{-3}$ μm$^{-2}$ (e.g., $N_s = 3 \times 10^{-3}$ μm$^{-2}$ is obtained from Fig. 2(a)). Thus, the mean next neighbor distance of surface crystals ($2l \sim N_s^{-1/2}$) is about 20 μm. Using the experimental crystal growth velocity (≈1 μm/h at 860°C), neighbor crystals will impinge after about 10 h. This impingement time is close to the observed time lag of the linear surface layer growth, $\tau_s \approx 11$ h (Fig. 4).

The measured nucleation densities, $N_s$, of *fractured* surfaces have a great deal of scatter, between $10^{-3}$ and $10^{-8}$ μm$^{-2}$ [29]. Assuming an intermediate $N_s \approx 10^{-5}$ μm$^{-2}$ (the corresponding next-neighbor distance of surface crystals of about 300 μm) and the experimental growth rate (78 μm/h at 980°C), the time for crystal impingement is about 2 h. This time is close to the time lag of layer growth for the fractured surface, $\tau_s$ (Fig. 5).

In another (endorsing) experiment, the crystallized surface fraction, $X_s$, was measured immediately following the apparent induction time for the surface layer growth at 860°C and 910°C (Table 2) for unpolished, as-received, glass surfaces. $X_s(\tau_s)$ was about 0.5 in both cases. Since our previous specimens (for which the crystal growth kinetics were determined) were polished by $CeO_2$, the fractional area crystallized for unpolished samples may be somewhat different, owing to a different number of nucleation sites on the surface [1–5,29]. However, an estimate of the crystallized surface area of the $CeO_2$ polished surfaces, using the Jonhson–Mehl–Avrami–Kolmogorov (JMAK) theory and the *experimental* $N_s$ and $U$, indicate that $0.3 < X_s < 0.7$. In addition, the fact that we could not continue to measure the growth velocity of the isolated crystals after 11 h of treatment reinforces this (impingement) argument.

Despite uncertainty regarding the precise crystallized surface areas, after a certain critical fraction of the surface is covered by crystals, impingement triggers a change in the growth

Table 2
Apparent induction times for growth of the crystallized layer towards the interior of GM 30870 glass, $\tau_s$, and crystallized fractional surface area, $X_s$, at the time $t = \tau_s$ for various temperatures

| $T$ (°C) | $\tau_s$ (h) | $X_s(\tau_s)$ |
|---|---|---|
| 860 | 11 ± 1 | 0.5 ± 0.1 |
| 880[a] | 4.2 | 0.3 – 0.7[a] |
| 900[a] | 1.8 | 0.3 – 0.7[a] |
| 910 | 1.3 ± 0.3 | 0.5 ± 0.1 |
| 920 | ≈0 | 0.0 |

[a] Estimated by the JMAK equation.

mode. Therefore, we infer that for treatments shorter than the impingement time, the surface crystals grow mainly in the lateral direction and the growth velocity is determined by $L_1$. Optical micrographs indeed show that a substantial fraction of the crystals are oriented with the $c_0$-axes parallel to the surface-elongated crystals.

Interplay of growth of all crystals, of any orientation, results in the exclusion (from further growth towards the sample interior) of inappropriately oriented crystallites. The competition among neighboring crystals increases with increasing surface area transformed and reaches a maximum at full impingement; i.e., when a critical $X_s$ is reached. This competition leads to a selection of crystals, oriented with the fast growing $c_0$-axis normal to the growth front (the sample surface), and only these selected crystals can grow further. Consequently, the growth velocity of the surface layer (if one measures the most frequent elongated crystals) changes from a small value before impingement (growth velocity of the $a_0$ or $b_0$ axes) to the final $dL_s/dt$ given above (growth of the $c_0$-axis).

It should be emphasized that the growth velocity normal to the surface, determined by measuring $L_s(U_{L_s})$, is about half $U_{L_1}$. From the average crystal shape we estimated that the growth velocities of the two crystal dimensions ($a_0$- and $c_0$-axis) differ by a factor of $\approx 2$. Therefore, assuming this ratio, the surface layer intercept in Fig. 4 can be explained. In summary, the induction time for surface layer growth is due to the change in the growth mode when a critical coverage of the surface is reached.

## 5. Summary and conclusions

The linear displacement velocities of three typical growth fronts were measured to elucidate differences in the growth of different crystallization routes of a cordierite glass. The crystal growth velocities of crystals in the volume and of the surface layer in the glass volume, as well as of isolated crystals on the glass surface are equal, within experimental error. Therefore, the *mechanism* of molecular rearrangement at the crystal growth interface on the surface is the same as that in the interior of these glasses.

A fiber *texture* was spontaneously formed (without the aid of epitaxial growth, temperature gradients, stresses or any other external variable) in the surface layer with preferential alignment of the $c_0$-axes of the grains normal to the growth front. The texture dispersion angle decreased towards the interior of the glass, in accordance with evolutionary microstructural models.

The apparent induction times for isolated crystal growth in the interior and on the glass surface were 2 and 3 h, respectively. Calculations demonstrated that the transient period for nucleation is in the same order of magnitude, thus accounting for the apparent induction times for growth. The smaller induction period of internally nucleated crystals is due to more efficient nucleation of the internal nucleating sites than the surface sites.

A much longer *induction time* was observed for the crystallized surface layer than for the isolated (internal or surface) crystals. This behavior can be explained in the following way: for the surface layer, we initially measured the growth velocity of the slow $a_0$- and $b_0$-axes of crystals whose fast $c_0$-axes are parallel to the glass surface. During the impingement stage, a major fraction of the crystals are oriented in such a way. We propose that surface tension phenomena can increase this orientation during longer growth periods of unimpinged crystals. These same crystals grow parallel to the glass surface covering it after a certain time. When the crystallized surface area reaches a critical magnitude, impingement precludes further growth of the faster growing crystals, and only the crystals that are oriented with the $c_0$-axes normal to the surface continue to grow towards the specimen center, forming a crystallized layer. This change appears as an apparent induction period.

## Acknowledgements

The authors acknowledge Dr Ralf Keding and Professor C. Rüssel – FSUJ, Jena; Dr Vladimir Fokin – Institute of Silicate Chemistry, St. Petersburg, and Dr Ervino C. Ziemath – IF Unesp,

Rio Claro, for useful suggestions and critical comments. The investigation presented here is part of a cooperative effort of the Technical Committee 7 of the ICG to advance the understanding of surface crystallization of glass. We also express our appreciation of the financial support of CNPq (Grant No. 521603/94-3), DAAD/CAPES Probral 025/96), PRONEX (76.97.1018.00) and Fapesp (99/0871-2).

## References

[1] E.D. Zanotto, Ceram. Trans. 30 (1993) 65.
[2] E.D. Zanotto, J. Non-Cryst. Solids 129 (1991) 183.
[3] K. Heide, G. Völksch, C.H.R. Hanay, in: Proceedings of the 16th International Congress on Glass, Madrid, Boletin de la Sociedad Espanola de Cerámica y Vidrio 5, 1992, p. 111.
[4] N.S. Yuritsin, V.M. Fokin, A.M. Kalinina, V.M. Filipovich, Ceram. Trans. 30 (1993) 379.
[5] N. Diaz-Mora, PhD thesis, Universidade Federal de São Carlos, São Carlos, SP, Brazil, 1994 (in Portuguese).
[6] E.C. Ziemath, N. Diaz-Mora, E.D. Zanotto, Phys. Chem. Glasses 38 (1997) 1.
[7] H.J. Bunge, K.H. Punch, Z. Metallkd. 75 (1984) 124.
[8] T.J. Headley, R.E. Loehman, J. Am. Ceram. Soc. 67 (1984) 620.
[9] C.L. Liu, S. Komarneni, R. Roy, J. Am. Ceram. Soc. 75 (1992) 2665.
[10] U. Selvaraj, C.L. Liu, S. Komarneni, J. Am. Ceram. Soc. 74 (1991) 1387.
[11] K.H. Ashbee, J. Mater. Sci. 10 (1975) 911.
[12] D.I.H. Atkison, P.W. McMillan, J. Mater. Sci. 12 (1997) 443.
[13] B.R. Durschang, G. Carl, C. Rüssel, K. Marchetti, E. Roeder, Glastech. Ber. Glass Sci. Technol. 67 (1994) 171.
[14] K. Engel, G.H. Frischat, Texture Microstruct. 24 (1995) 155.
[15] G.J. Gardopee, R.E. Newnham, A.S. Bhalla, Ferroelectrics 33 (1981) 155.
[16] T. Rudolph, D.V. Szabo, W. Pannhorst, K.L. Weisskopf, G. Petzow, Glastech. Ber. 64 (1991) 218.
[17] M.D. Kharkhanavala, F.A. Hummel, J. Am. Ceram. Soc. 36 (1953) 389.
[18] W. Schreyer, J.F. Schairer, Z. Kristallogr. 116 (1961) 60.
[19] R. Müller, S. Reinsch, W. Pannhorst, Glastech. Ber. Glass Sci. Technol. 69 (1996) 11.
[20] R. Müller, L. Weh, S. Reinsch, Glastechnische Tagung, Halle/S 1999 (to be published).
[21] R. Hergt, H. Pfeiffer, L. Fritzsch, Phys. Stat. Sol. (a) 98 (1986) 69.
[22] R. Hergt, H. Pfeiffer, Phys. Stat. Sol. (a) 92 (1985) K89.
[23] I. Gutzow, J. Schmelzer, The Vitreous State, Springer, Berlin, 1995.
[24] A.V. Gorokhovskii, et al., Glass Phys. Chem. 20 (1994) 537.
[25] M.C. Weinberg, J. Non-Cryst. Solids 170 (1994) 300.
[26] R. Pascova, I. Penkov, I. Gutzow, Boletin de la Sociedad Espanola de Ceramica y Vidrio: 16th International Congress on Glass, Madrid, 2, 189.
[27] R. Müller, R. Naumann, S. Reinsch, Thermochim. Acta 280&281 (1996) 1919.
[28] V.M. Fokin, N.S. Yuritsin, A.M. Kalinina, V.N. Filipovich, Glastech. Ber. Glass Sci. Technol. C 67 (1994) 392.
[29] R. Müller, J. Non-Cryst. Solids 219 (1997) 110.